INTERNATIONAL JOURNAL FOR NUMERICAL METHODS IN FLUIDS, VOL. 23, 309–323 (1996)

FULLY DISCRETE HIGH-RESOLUTION SCHEMES FOR HYPERBOLIC CONSERVATION LAWS

J. SHI

Department of Civil Engineering, Queen Mary and Westfield College, Mile End Road, London, U.K.

AND

E. F. TORO

Department of Mathematics and Physics, Manchester Metropolitan University, Chests Street, Manchester, U.K.

SUMMARY

The present paper is a sequel to two previous papers in which rigorous, up to fourth-order, fully discrete (FD) upwind TVD schemes have been presented. In this paper we discuss in detail the extension of these schemes to solutions of non-linear hyperbolic systems. The performance of the schemes is assessed by solving test problems for the time-dependent Euler equations of gas dynamics in one and two space dimensions. We use exact solutions and experimental data to validate the results.

KEY WORDS: fully discrete; upwind scheme; TVD; high-order; hyperbolic

1. INTRODUCTION

In References 1 and 2, up to fourth-order FD upwind schemes have been obtained. In this paper a way to extend the previous work to general systems of non-linear hyperbolic conservation laws is discussed in detail.

For constant coefficient linear hyperbolic systems the extension is straightforward. Recall that these FD schemes are high-resolution upwind schemes and can accommodate arbitrary wave directions, so they can automatically deal with linear systems of equations with eigenvalues of mixed sign. For non-linear hyperbolic systems, however, the matrix of eigenvalues is not constant, which means that the numerical flux cannot be defined directly. Hence the approach for linear systems no longer holds when solving non-linear systems. Godunov[3] provided a way of dealing with non-linear systems. Rather than diagonalizing the Jacobian matrix, Godunov's method employs the solutions of Riemann problems which can be computed exactly and give substantial information about the local characteristic structure. Following Godunov's approach, the high-resolution numerical fluxes developed in previous papers could be defined by solving Riemann problems.

In this paper we first discuss the extension of the high-resolution schemes to linear systems and then extend the discussion to non-linear systems of conservation laws. To illustrate the methodology, a family of up to fourth-order upwind schemes for systems of non-linear hyperbolic conservation laws is presented. These schemes are validated by applications to the time-dependent Euler equations in one and two dimensions.

CCC 0271–2091/96/040309–15

Received August 1995
Revised November 1995

The rest of the paper is organized as follows. Section 2 briefly reviews the fully discrete high-resolution schemes for the scalar case. Section 3 extends the schemes to linear systems. Section 4 discusses non-linear systems, typically the time-dependent Euler equations of gas dynamics. Section 5 reports the numerical experiments. Section 6 draws conclusions.

2. A FAMILY OF HIGH-ORDER UPWIND TVD SCHEMES

For continuity, in this section we briefly review a family of up to fourth-order FD upwind TVD schemes introduced in References 1 and 2.

The family of upwind TVD schemes can be written in a general finite volume form as

$$U_j^{n+1} = U_j^n - \frac{k}{h}\left(F_{j+1/2} - F_{j-1/2}\right), \tag{1}$$

$$F_{j+1/2} = \tfrac{1}{2}(F_j^n + F_{j+1}^n) - \tfrac{1}{2}|a|\Delta U_{j+1/2} + |a|\left(D_0\Delta U_{j+1/2} + D_1\Delta U_{j+L+1/2}\right)\phi_j + |a|D_2\Delta U_{j+M+1/2}\phi_{j+M}, \tag{2}$$

where $h = \Delta x$ is a uniform mesh width and $k = \Delta t$ is a time step. D_0, D_1 and D_2 are coefficients; ϕ_j and ϕ_{j+M} are limiter functions;

$$\Delta U_{j+q+1/2} = U_{j+q+1}^n - U_{j+q}^n \quad (q = 0, L, M), \tag{3}$$

$$\begin{aligned} &L = -1 \quad \text{and} \quad M = 1 \quad \text{for } c > 0, \\ &L = 1 \quad \text{and} \quad M = -1 \quad \text{for } c < 0, \end{aligned} \tag{4}$$

where c is a Courant number. The above formula includes three-point second-order stencil-centred schemes, five-point second-order stencil-upwind schemes, five-point third-order stencil-upwind-biased schemes and five-point fourth-order stencil-centred schemes. For example, when

$$D_1 = D_2 = 0, \qquad D_0 = (1 - |c|)/2, \tag{5}$$

the second-order stencil-centred scheme is obtained which has the stability condition $|c| \leqslant 1$; when

$$D_0 = D_2 = 0, \qquad D_1 = (1 - |c|)/2, \tag{6}$$

this gives the second-order stencil-upwind scheme which has the stability condition $|c| \leqslant 2$; when

$$D_2 = 0, \qquad D_1 = (1 - c^2)/6, \qquad D_0 = 1/3 - |c|/2 + c^2/6, \tag{7}$$

the five-point third-order stencil-upwind-biased scheme is obtained which has the stability condition $|c| \leqslant 1$; when

$$\begin{aligned} D_0 &= 1/2 - 7|c|/12 + |c^3|/12, \\ D_1 &= 1/12 + |c|/24 - c^2/12 - |c^3|/24, \\ D_2 &= c^2/12 + |c|/24 - 1/12 - |c^3|/24, \end{aligned} \tag{8}$$

the five-point fourth-order stencil-centred scheme is obtained which has the stability condition $|c| \leqslant 1$. The flux limiter functions can be defined as

$$\phi_j = \begin{cases} \dfrac{(1-|c|)\theta_j}{\eta(D_1\theta_j + D_0 - D_2)} & \text{for } 0 \leqslant \theta_j < \theta^{\mathrm{L}}, \\ 1 & \text{for } \theta^{\mathrm{L}} \leqslant \theta_j \leqslant \theta^{\mathrm{R}}, \\ \dfrac{1-|c|+\eta D_2 \phi_{j+M}/\theta_j^*}{\eta(D_0 + D_1\theta_j)} & \text{for } \theta_j > \theta^{\mathrm{R}}, \\ 0 & \text{for } \theta_j < 0, \end{cases} \tag{9}$$

$$\phi_{j+M} = \begin{cases} \eta\theta_{j+M} & \text{for } 0 \leqslant \theta_{j+M} < 0{\cdot}5, \\ 1 & \text{for } \theta_{j+M} > 0{\cdot}5, \\ 0 & \text{for } \phi_j = 0, \end{cases} \tag{10}$$

where

$$\theta^{\mathrm{L}} = \frac{\eta(D_0 - D_2)}{1-|c|-\eta D_1}, \qquad \theta^{\mathrm{R}} = \frac{1-|c|-\eta(D_0 - D_2\phi_{j+M}/\theta_j^*)}{\eta D_1}, \tag{11}$$

θ_j is the local flow parameter defined by

$$\theta_j = \begin{cases} \Delta U_{j-1/2}/\Delta U_{j+1/2} & \text{for } c > 0, \\ \Delta U_{j+3/2}/\Delta U_{j+1/2} & \text{for } c < 0, \end{cases} \tag{12}$$

θ_j^* is the upwind–downwind flow parameter given by

$$\theta_j^* = \begin{cases} \Delta U_{j-1/2}/\Delta U_{j+3/2} & \text{for } c > 0, \\ \Delta U_{j+3/2}/\Delta U_{j-1/2} & \text{for } c < 0, \end{cases} \tag{13}$$

and η is defined by

$$\eta = \begin{cases} 1-|c| & \text{for } 0 \leqslant |c| < \frac{1}{2}, \\ |c| & \text{for } \frac{1}{2} \leqslant |c| \leqslant 1. \end{cases} \tag{14}$$

3. LINEAR HYPERBOLIC SYSTEMS

In this section we extend the scalar schemes (1), (2) to solve the initial value problem for linear hyperbolic systems with constant coefficients:

$$U_t + AU_x = 0, \qquad U(x,0) = U_0(x), \tag{15}$$

where U is a column vector of m conserved variables and A is an $m \times m$ constant matrix.

This is a system of conservation laws with the flux function $F(u) = AU$ which is hyperbolic if A is diagonalizable with real eigenvalues, i.e. the matrix A can be written as

$$A = R\Lambda R^{-1} \tag{16}$$

where $\Lambda = \mathrm{diag}(\lambda^{(1)}, \lambda^{(2)}, \ldots, \lambda^{(m)})$ is the diagonal matrix of eigenvalues of A and $R = (r^{(1)}, r^{(2)}, \ldots, r^{(m)})$ is the matrix of right eigenvectors of A.

Equation (16) means $AR = R\Lambda$, i.e.

$$Ar^{(p)} = \lambda^{(p)} r^{(p)}, \quad p = 1, 2, \ldots, m. \tag{17}$$

The natural way to extend the scalar schemes to linear systems is obtained by defining expressions for the flux differences $\Delta F_{j+1/2} = A\Delta U_{j+1/2}$. This can be done by diagonalizing the system, solving local Riemann problems with left and right states U_j^n and U_{j+1}^n, i.e.

$$U(x,0) = \begin{cases} U_j^n, & x<0, \\ U_{j+1}^n, & x>0, \end{cases} \tag{18}$$

and letting

$$\alpha_{j+1/2} = R_{j+1/2}^{-1}\Delta U_{j+1/2}, \tag{19}$$

where $R_{j+1/2}$ is the matrix of right eigenvectors at the interface $j+\frac{1}{2}$, which for the linear constant coefficient case is of course constant; $\alpha_{j+1/2}$ is called the wave strength vector with components $\alpha_{j+1/2}^{(p)}$ $(p = 1, 2, \ldots, m)$ across the pth wave travelling at speed $\lambda_{j+1/2}^{(p)}$ in the $(j+\frac{1}{2})$ intercell. Then we have

$$\Delta U_{j+1/2} = \sum_{p=1}^{m} \alpha_{j+1/2}^{(p)} r_{j+1/2}^{(p)}. \tag{20}$$

Since $F(U) = AU$, this leads to

$$\begin{aligned} \Delta F_{j+1/2} &= A\Delta U_{j+1/2} \\ &= \sum_{p=1}^{m} \alpha_{j+1/2}^{(p)} A r_{j+1/2}^{(p)} \\ &= \sum_{p=1}^{m} \alpha_{j+1/2}^{(p)} \lambda_{j+1/2}^{(p)} r_{j+1/2}^{(p)}. \end{aligned} \tag{21}$$

Note that the single jump $\Delta F_{j+q+1/2} = |a_{j+q+1/2}|\Delta U_{j+q+1/2}$ in the scalar scheme (2), with the appropriate interpretation for $|a_{j+1/2}|$, is now substituted by a summation of jump (21), which gives a natural extension to linear systems with constant coefficients.

4. NON-LINEAR HYPERBOLIC SYSTEMS

In this section we discuss the extension of the scalar schemes (1), (2) to two-dimensional non-linear systems of conservation laws, but the same ideas can be applied in three dimensions as well. The Euler equations are taken as a typical non-linear system of conservation laws to develop the presentation on how to extend our schemes.

4.1. Euler equations

The two-dimensional Euler equations of gas dynamics are

$$U_t + F(U)_x + G(U)_y = 0, \tag{22}$$

where

$$U = \begin{pmatrix} \rho \\ \rho u \\ \rho v \\ E \end{pmatrix}, \qquad F(U) = \begin{pmatrix} \rho u \\ \rho u^2 + p \\ \rho uv \\ u(E+p) \end{pmatrix}, \qquad G(U) = \begin{pmatrix} \rho u \\ \rho uv \\ \rho v^2 + p \\ v(E+p) \end{pmatrix}, \tag{23}$$

$$p = (\lambda - 1)[E - \tfrac{1}{2}\rho(u^2 + v^2)]. \tag{24}$$

Here ρ, u, v, ρu, ρv, p and E are the density, x- and y-direction velocities, x- and y-direction momenta, pressure and total energy respectively; γ is the ratio of specific heats.

For the split one-dimensional problem the eigenvalues of the Jacobian matrix $F'(U)$ are

$$\lambda^{(1)} = u - a, \qquad \lambda^{(2)} = \lambda^{(3)} = u, \qquad \lambda^{(4)} = u + a. \tag{25}$$

The corresponding right eigenvectors are

$$r^{(1)} = \begin{pmatrix} 1 \\ u-a \\ v \\ h-ua \end{pmatrix}, \quad r^{(2)} = \begin{pmatrix} 1 \\ u \\ v \\ \frac{1}{2}(u^2+v^2) \end{pmatrix}, \quad r^{(3)} = \begin{pmatrix} 0 \\ 0 \\ 1 \\ v \end{pmatrix}, \quad r^{(4)} = \begin{pmatrix} 1 \\ u+a \\ v \\ h+ua \end{pmatrix}, \tag{26}$$

where h is the specific enthalpy given by

$$h = \frac{E+p}{\rho} \tag{27}$$

The eigenvalues of the Jacobian matrix $G'(U)$ have the same form but the roles of u and v are interchanged.

One popular approach to solving multidimensional problems is to apply the method of *fractional steps* or *operator splitting*.[4] In this approach the 2D system (22) is split into two augmented one-dimensional systems, then the solution of (22) is obtained by solving the two 1D problems sequentially. In this paper the Strang splitting method will be used to deal with 2D problems. Therefore from now on we turn our attention to studying one-dimensional non-linear systems.

4.2. *Godunov's method*

From the nature of non-linear systems the eigenvalues are functions of the unknowns, which means that we cannot explicitly define the intercell flux $F_{j+1/2}$ as in the case of linear systems. To deal with the problem, Godunov provided a way of utilizing the solution of the Riemann problem with left and right states U_j^n and U_{j+1}^n.[3] Thus the Godunov flux can be written as

$$F_{j+1/2}^{\mathrm{G}} = F\big(u_{j+1/2}^*(U_j^n, U_{j+1}^n)\big), \tag{28}$$

where $u_{j+1/2}^*(U_j^n, U_{j+1}^n)$ are the cell interface values at $x_{j+1/2}$. However, Godunov's method is only first-order-accurate. To obtain higher-order accuracy, more grid points are needed, which results in more interface values $u_{j+m+1/2}^*$ involved in the high-order numerical fluxes

$$F_{j+1/2}^{\mathrm{H}} = F\big(u_{j+m+1/2}^*(U_{j+m}^n, U_{j+m+1}^n)\big), \tag{29}$$

where $m = 0, \pm 1, \pm 2, \ldots$ are integers according to a specific scheme. For scheme (2), for example, the flux is

$$F_{j+1/2} = F\big(u_{j-1/2}^*(U_{j-1}^n, U_j^n), u_{j+1/2}^*(U_j^n, U_{j+1}^n), u_{j+3/2}^*(U_{j+1}^n, U_{j+2}^n)\big). \tag{30}$$

There are essentially two ways of obtaining the values of u^* and hence the intercell flux $F_{j+1/2}$ utilizing a Riemann problem solution. One way is to obtain the flux function directly. For non-linear systems this is always an approximate procedure. We called this the *flux Riemann problem approach* (flux Riemann solver). Another way is to find the solution of the Riemann problem for the state variables u^* and then the intercell flux can be obtained by evaluating the physical flux function, i.e. $F_{j+1/2} = F(u^*)$. The solution u^* can be approximate or exact. We call this the *state Riemann problem approach* (state Riemann solver).

4.3. Flux Riemann solvers

A possible strategy for solving systems of non-linear conservation laws is to linearize the non-linear system of equations (22) locally at each cell interface by an approximate Riemann solver and then implement the methods of the last section using the linearized systems

$$U_t + \bar{A}U_x = 0, \tag{31}$$

where $\bar{A}$ is a linearized constant matrix depending only on the local data U_j^n and U_{j+1}^n, i.e. $\bar{A} = \bar{A}(U_j^n, U_{j+1}^n)$.

Popular examples of this approach are Roe's Riemann solver[5] and Engquist's Riemann solver.[6] Roe's matrix $\bar{A}(U_j^n, U_{j+1}^n)$ is assumed to satisfy the following properties: (i) $\bar{A}\Delta U_{j+1/2} = \Delta F_{j+1/2}$; (ii) $\bar{A}$ is diagonalizable with real eigenvalues; (iii) $A \to f'(\bar{U})$ smoothly as U_j^n, $U_{j+1}^n \to \bar{U}$. Denoting the Roe eigenvalues, eigenvectors and wave strengths as $\tilde{\lambda}_{j+1/2}^{(p)}$, $\tilde{r}_{j+1/2}^{(p)}$ and $\tilde{\alpha}_{j+1/2}^{(p)}$ $(p = 1,2,\ldots,m)$ respectively, then applying the high-order schemes of the last section, we solve the original non-linear systems in a straightforward manner.

The Roe eigenvalues and eigenvectors are evaluated at the average state $\bar{U}$, which for the one-dimensional case takes the form

$$\begin{aligned} \tilde{u} &= (\rho_j^{1/2}u_j + \rho_{j+1}^{1/2}u_{j+1})/(\rho_j^{1/2} + \rho_{j+1}^{1/2}), & \tilde{\rho} &= (\rho_j\rho_{j+1})^{1/2}, \\ \tilde{h} &= (\rho_j^{1/2}h_j + \rho_{j+1}^{1/2}h_{j+1})/(\rho_j^{1/2} + \rho_{j+1}^{1/2}), & \tilde{a} &= [(\gamma-1)(\tilde{h} - \tfrac{1}{2}\tilde{u}^2)]^{1/2}. \end{aligned} \tag{32}$$

The average wave strengths $\tilde{\alpha}^{(p)}$ are determined by

$$\tilde{\alpha}^{(1)} = \frac{1}{2\tilde{a}^2}(\Delta p - \tilde{\rho}\tilde{a}\Delta u), \qquad \tilde{\alpha}^{(2)} = \Delta\rho - \frac{\Delta p}{\tilde{a}^2}, \qquad \tilde{\alpha}^{(3)} = \frac{1}{2\tilde{a}^2}(\Delta p + \tilde{\rho}\tilde{a}\Delta u), \tag{33}$$

where

$$\Delta\rho = \rho_{j+1} - \rho_j, \qquad \Delta u = u_{j+1} - u_j, \qquad \Delta p = p_{j+1} - p_j. \tag{34}$$

However, it is well known that under some circumstances Roe's Riemann solver can admit non-physical solutions such as expansion shocks and negative densities. The first failure is due to the fact that Roe's Riemann solver does not satisfy an entropy condition.[7] To remedy this, a sonic fix is required. There are several entropy fixes in the literature. In this paper we apply one introduced by Harten and Hyman.[8] The second failure afflicts all linearized Riemann solvers. Possible cures for this difficulty were studied in Reference 9.

4.4. State Riemann solvers

These solvers include exact solvers and hybrid solvers which solve the Riemann problem for the state variables. For example, Toro's hybrid solver[10] includes a linearized solver and an exact solver which are used adaptively. The switch between the two solvers is governed by a simple mechanism. Applications of this hybrid solver show that about 98% of all Riemann problems are solved by the fast linearized solver and only in the case of energetic flows does the exact solver take over. The structure of the solution of the Riemann problem contains two intermediate regions between the two non-linear waves. They are separated by the contact wave and we use the notation q_L^* and q_R^* for quantities to the left and right of the contact respectively.

The 'star values' obtained locally by the linearized solver in one dimension have the form

$$\begin{aligned} u^* &= \tfrac{1}{2}(u_j + u_{j+1}) - (p_{j+1} - p_j)/2\bar{\rho}\bar{a}, & p^* &= \tfrac{1}{2}(p_u + p_{j+1}) - \tfrac{1}{2}\bar{\rho}\bar{a}(u_{j+1} - u_j), \\ \rho_L^* &= \rho_j + (u_j - u^*)\bar{\rho}/\bar{a}, & \rho_R^* &= \rho_{j+1} + (u^* - u_{j+1})\bar{\rho}/\bar{a}, \end{aligned} \tag{35}$$

where

$$\bar{\rho} = \tfrac{1}{2}(\rho_j + \rho_{j+1}), \qquad \bar{a} = \tfrac{1}{2}(a_j + a_{j+1}) \tag{36}$$

are the average values of the density and sound speed respectively.

Once the 'star values' at each cell interface have been calculated, the flux jump $\Delta F_{j+1/2}^{(p)}$ for each wave can be easily defined. Then, applying the high-order upwind schemes (see next subsection), we solve the non-linear systems to high-order accuracy.

4.5. *Upwind schemes for non-linear systems*

Taking Roe's Riemann solver for Euler equations, for instance, scheme (2) can be extended to solve non-linear systems as

$$\begin{aligned} F_{j+1/2} = {} & \tfrac{1}{2}(F_j^n + F_{j+1}^n) - \tfrac{1}{2}\sum_{p=1}^{m} |\bar{\lambda}_{j+1/2}^{(p)}| \bar{\alpha}_{j+1/2}^{(p)} \bar{r}_{j+1/2}^{(p)} \\ & + \sum_{p=1}^{m} \left(D_{j+1/2}^{(p)} |\bar{\lambda}_{j+1/2}^{(p)}| \bar{\alpha}_{j+1/2}^{(p)} \bar{r}_{j+1/2}^{(p)} + D_{j+L+1/2}^{(p)} |\bar{\lambda}_{j+L+1/2}^{(p)}| \bar{\alpha}_{j+L+1/2}^{(p)} \bar{r}_{j+L+1/2}^{(p)} \right) \phi_j^{(p)} \\ & + D_{j+M+1/2}^{(p)} |\bar{\lambda}_{j+M+1/2}^{(p)}| \bar{\alpha}_{j+M+1/2}^{(p)} \bar{r}_{j+M+1/2}^{(p)} \phi_{j+M}^{(p)}, \end{aligned} \tag{37}$$

where $\bar{\lambda}^{(p)}$, $\bar{r}^{(p)}$ and $\bar{\alpha}^{(p)}$ $(p = 1, 2, \ldots, m)$ are the Roe-averaged eigenvalues, eigenvectors and wave strengths respectively across the pth wave at cell interfaces, $D^{(p)} = f(c^{(p)})$ are functions of the cell Courant number (see (5)–(8)) and $\phi^{(p)} = f(c^{(p)}, \theta^{(p)})$ are limiter functions (see (9)–(14)).

5. NUMERICAL EXPERIMENTS

In this section we report numerical experiments with the fully discrete second-order scheme (5), third-order scheme (7) and fourth-order scheme (8). Details of the limiters used in the paper, i.e. FD2A, FD2B, FD3A, FD3B, FD4A and FD4B, can be found in Reference 2. Four test problems are considered.

5.1. *Entropy test problem*

Here we choose a sonic test problem with initial data

$$(\rho, u, p) = \begin{cases} (1, 0{\cdot}75, 1), & 0 \leqslant x \leqslant 0{\cdot}5, \\ (0{\cdot}125, 0, 0{\cdot}1), & 0{\cdot}5 < x \leqslant 1{\cdot}0. \end{cases} \tag{38}$$

This problem is a modification of Sod's problem and is designed to produce a left sonic rarefaction at about $x = 0{\cdot}5$. Therefore it is a good problem to test the entropy-satisfying property of a numerical scheme.

Figures 1 and 2 show the performance of our schemes. The computational domain is divided into 100 computational cells. The Courant number used is 0·8. The full line is the exact solution and the symbols are the numerical result. Figures 1(a)–1(c) show the results obtained by the second-, third- and fourth-order schemes respectively with Roe's solver without entropy fixing. As clearly seen, the second-order scheme (a) automatically satisfies the entropy condition, whereas the solutions of the third and fourth

order schemes (b) and (c) contain a rarefaction shock which is unphysical. Figure 2 shows the corresponding results obtained with Harten and Hyman's entropy fix.[8] The entropy-satisfying condition of the third- and fourth-order schemes is obviously improved.

5.2. *Sod's problem*

Sod's problem[11] is one of the most popular test problems for numerical schemes. Therefore we chose this problem to test all our limiters presented in the previous sections. Sod's problem consists of initial data

$$(\rho, u, p) = \begin{cases} (1, 0, 1), & 0 \leqslant x \leqslant 0{\cdot}5, \\ (0{\cdot}125, 0, 0{\cdot}1), & 0{\cdot}5 < x \leqslant 1{\cdot}0. \end{cases} \tag{39}$$

Figures 3–8 show the comparison between the computed results (symbols) and the exact solution (full line) with Roe's Riemann solver at time 0·2 units. Again we used 100 cells and 0·8 for the Courant number. Figure 3 shows the performance of the second-order scheme with the FD2A limiter. As seen in the figure, the numerical results look satisfactory in the smooth parts. The shocks are captured with two to three interior points, but the contact discontinuities are smeared with four to five points. There are no overshoots or undershoots.

Figure 4 shows the results of the second-order scheme with the FD2B limiter. Comparing with the results obtained with the FD2A limiter (see Figure 3), the FD2B limiter shows an obvious improvement in capturing the contacts with two to three points; however, there are overshoots and undershoots, especially in the internal energy plot (d).

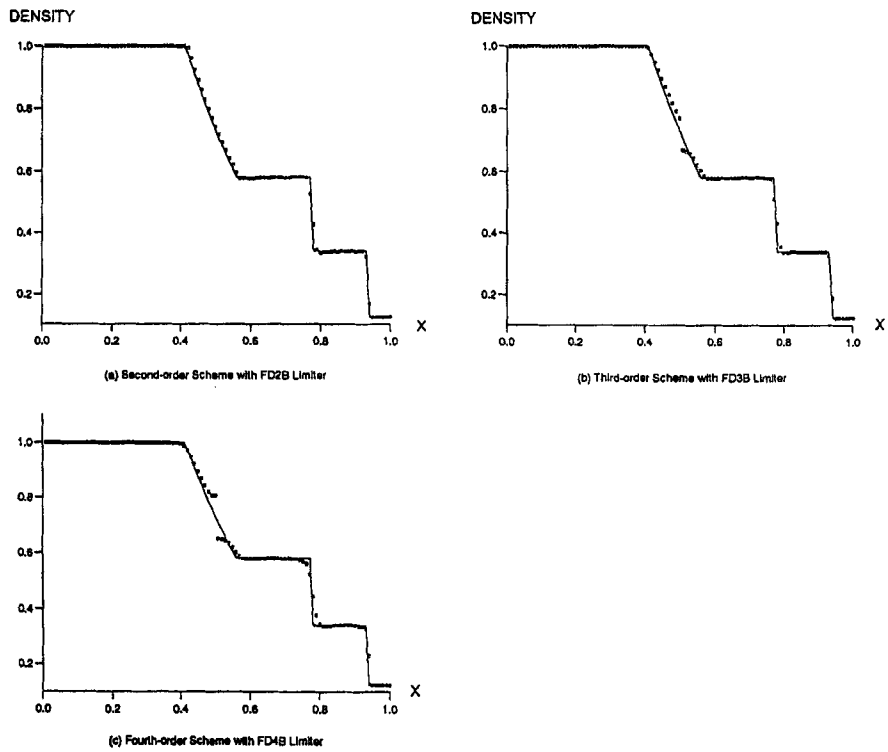

Figure 1. Entropy test problem without entropy fixing by second-, third- and fourth-order schemes

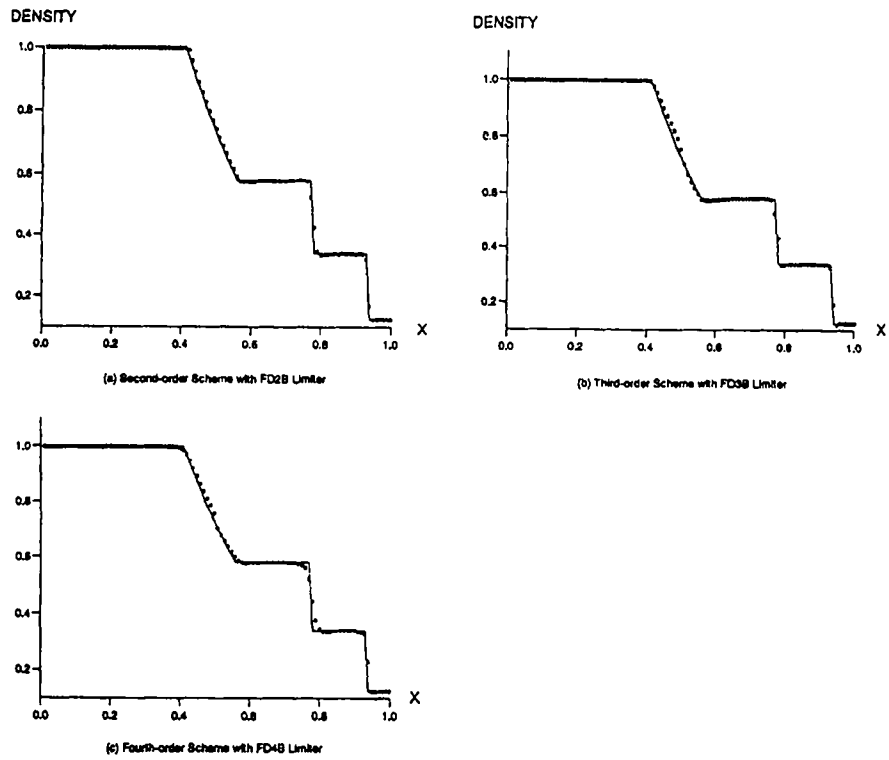

Figure 2. Entropy test problem with entropy fixing by second-, third- and fourth-order schemes

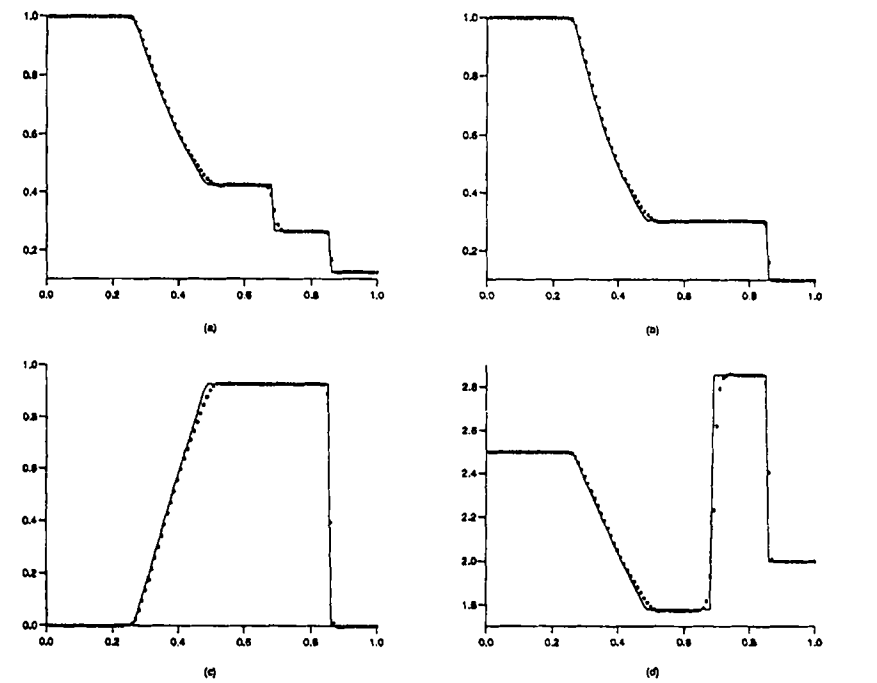

Figure 3. Sod's problem by second-order scheme with FD2A limiter: (a) density; (b) pressure; (c) velocity; (d) energy

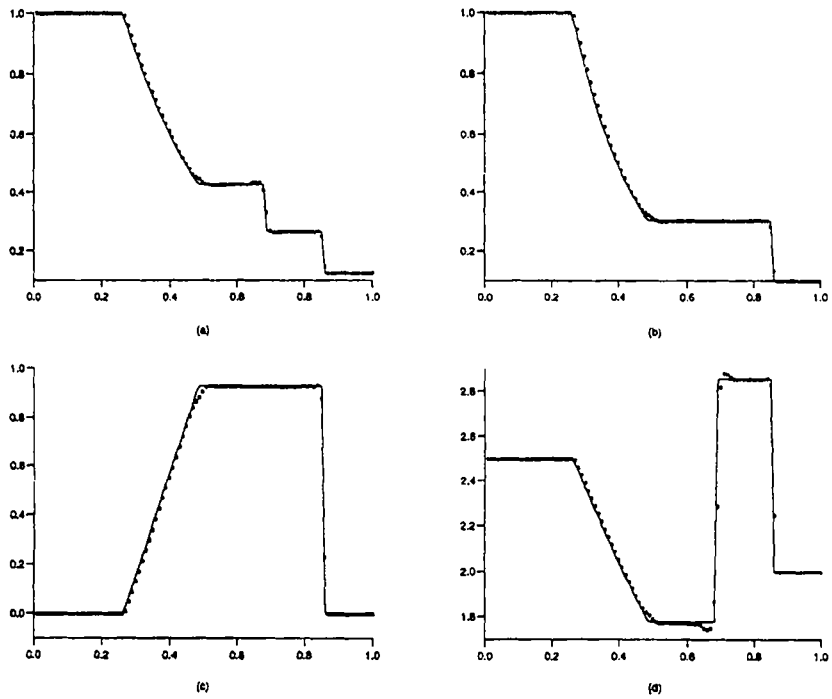

Figure 4. Sod's problem by second-order scheme with FD2B limiter; (a) density; (b) pressure; (c) velocity; (d) energy

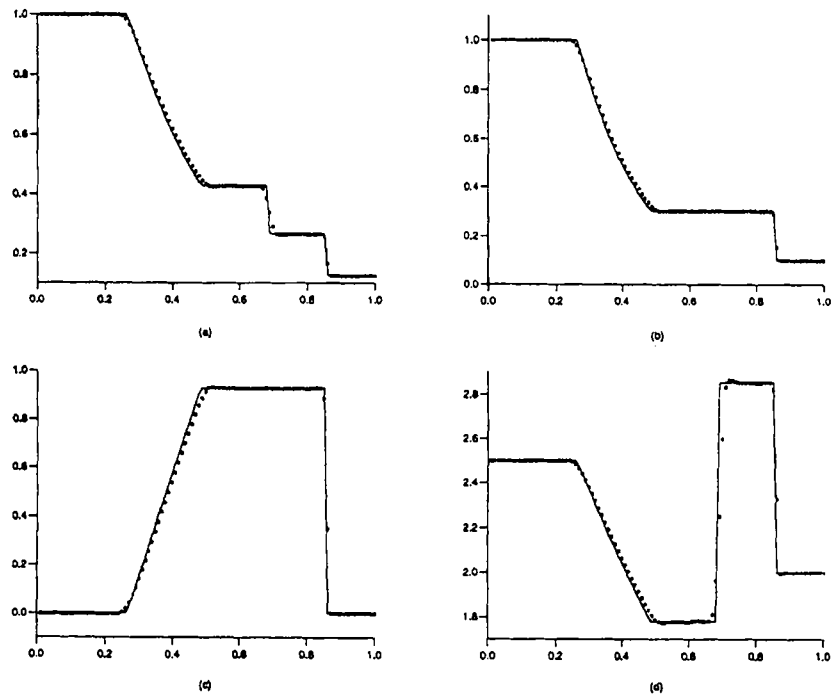

Figure 5. Sod's problem by third-order scheme with FD3A limiter: (a) density; (b) pressure; (c) velocity; (d) energy

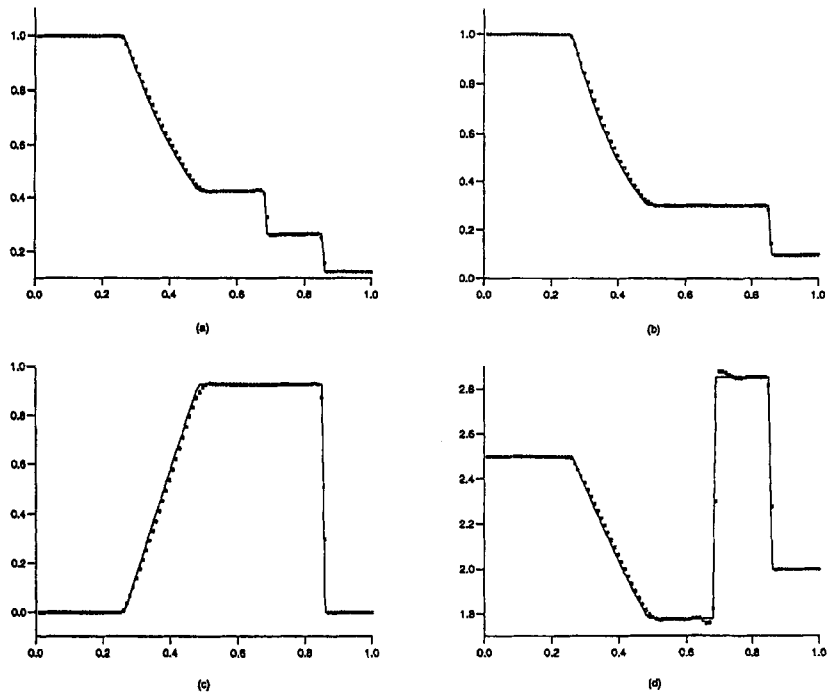

Figure 6. Sod's problem by third-order scheme with FD3B limiter: (a) density; (b) pressure; (c) velocity; (d) energy

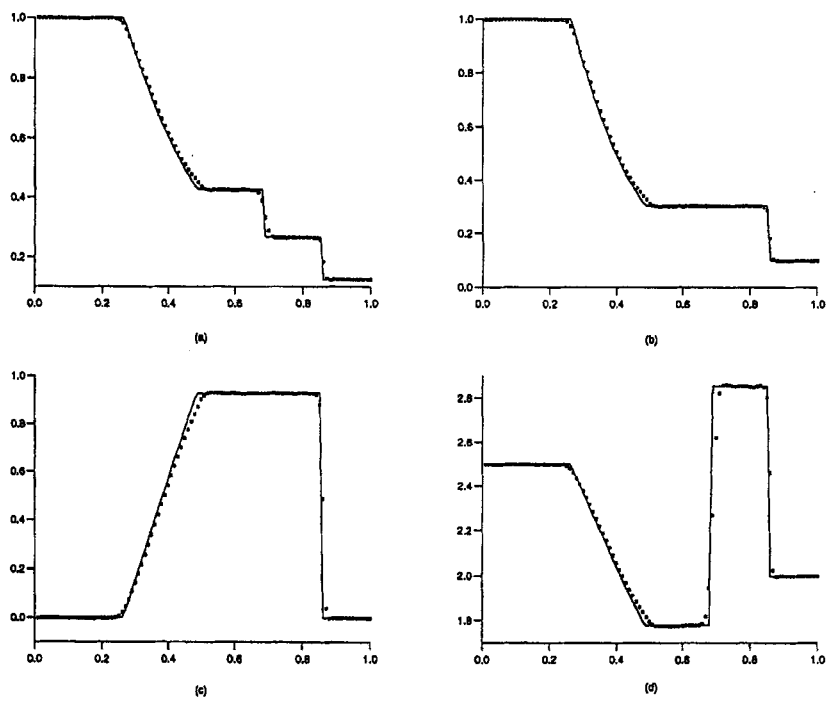

Figure 7. Sod's problem by fourth-order scheme with FD4A limiter: (a) density; (b) pressure; (c) velocity; (d) energy

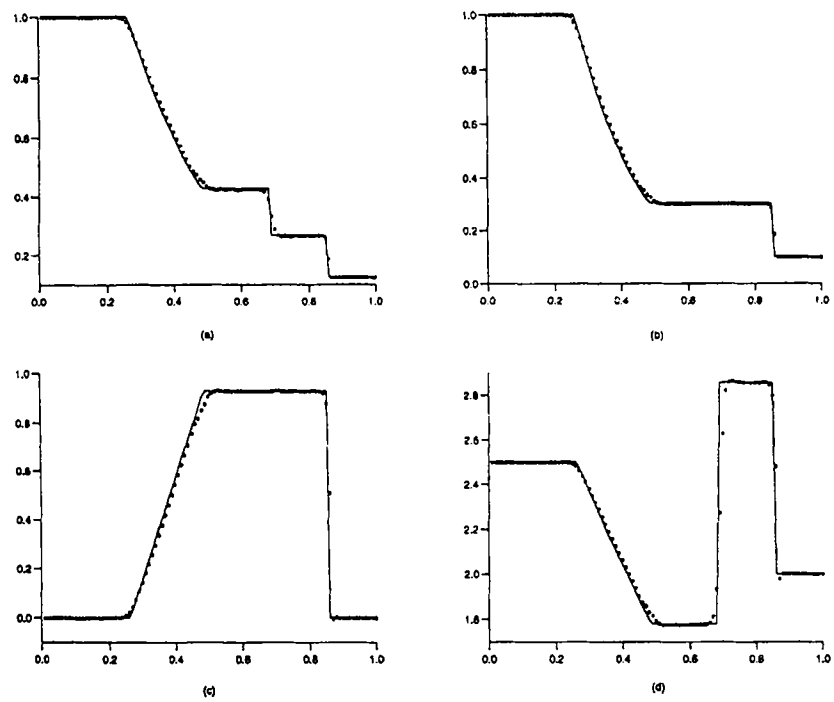

Figure 8. Sod's problem by fourth-order scheme with FD4B limiter: (a) density; (b) pressure; (c) velocity; (d) energy

Figure 5 shows the results obtained by the third-order scheme with the FD3A limiter. The results look very satisfactory for both smooth parts and shocks. However, the contact has four to five points and there is a very little overshoot in the energy (d).

Figure 6 shows the performance of the third-order scheme with the FD3B limiter. Except for a few overshoots and undershoots, the results of the limiter are very satisfactory. Both shocks and contacts are captured with only two points. The overall performance of the third-order scheme is superior to that of the second-order scheme (compare Figures 5 and 6 with Figures 3 and 4).

Figure 7 shows the numerical results of the fourth-order scheme with the FD4A limiter. The smooth part of the solution is good; the shocks are captured with three points and the contacts with five points. Very small oscillations can be seen. It is generally accepted that designing a proper dissipation procedure for high-order methods is a very difficult task. We are satisfied with the performance observed.

Figure 8 shows the solution of the fourth-order scheme with the FD4B limiter. The results are superior to those obtained with the FD4A limiter (see Figure 7). Both shocks and contacts are presented with three points. Also, the FD4B limiter is simpler than FD4A. The overall performance of the fourth-order scheme is better than that of the third-order scheme (compare Figures 7 and 8 with Figures 5 and 6).

5.3. Blast wave problem

The blast wave problem introduced by Woodward and Collela[12] is a severe test problem and therefore a good problem to test the robustness of numerical schemes. This problem has initial data

$$(\rho, u, p) = \begin{cases} (1, 0, 1000), & 0 \leqslant x < 0{\cdot}1, \\ (1, 0, 0{\cdot}1), & 0{\cdot}1 \leqslant x < 0{\cdot}9, \\ (1, 0, 100), & 0{\cdot}9 \leqslant x \leqslant 1{\cdot}0. \end{cases} \tag{40}$$

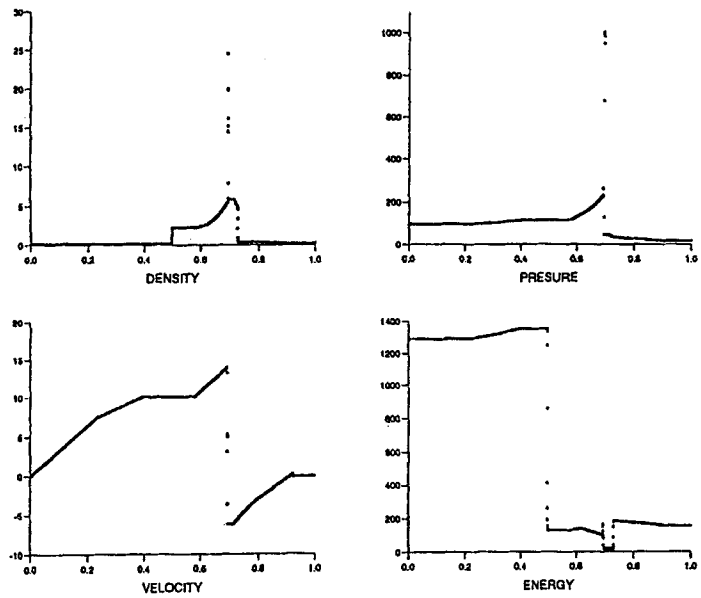

Figure 9. Blast wave problem by second-order scheme with FD2B limiter

Although there is no exact solution for this test problem, there are several good numerical results available. We discretize the domain with 3000 cells. The Courant number used is 0·8. We applied a hybrid scheme involving Roe's solver and an exact solver used adaptively. We chose the second-order scheme with the FD2B limiter, third-order with FD3B and fourth-order with FD4B to test the robustness of the high-order schemes. Figures 9–11 show the numerical results at time 0·028. The results show that the schemes reproduce accurately the known features of the solution.

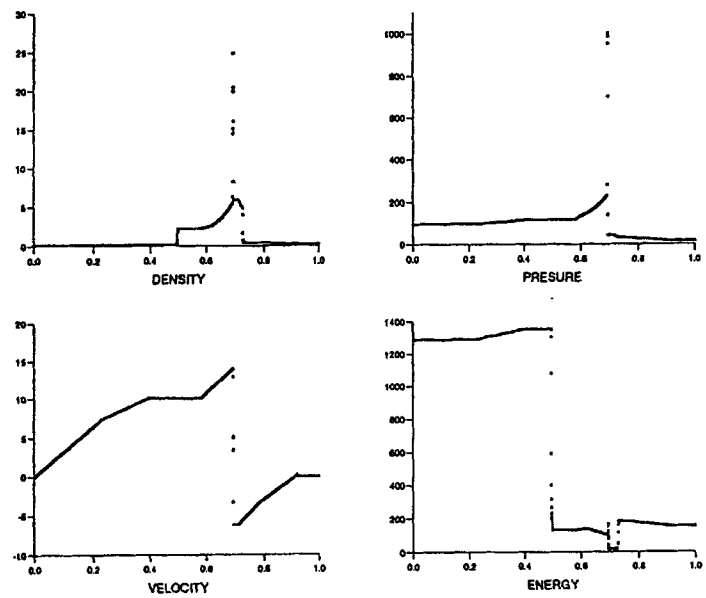

Figure 10. Blast wave problem by third-order scheme with FD3B limiter

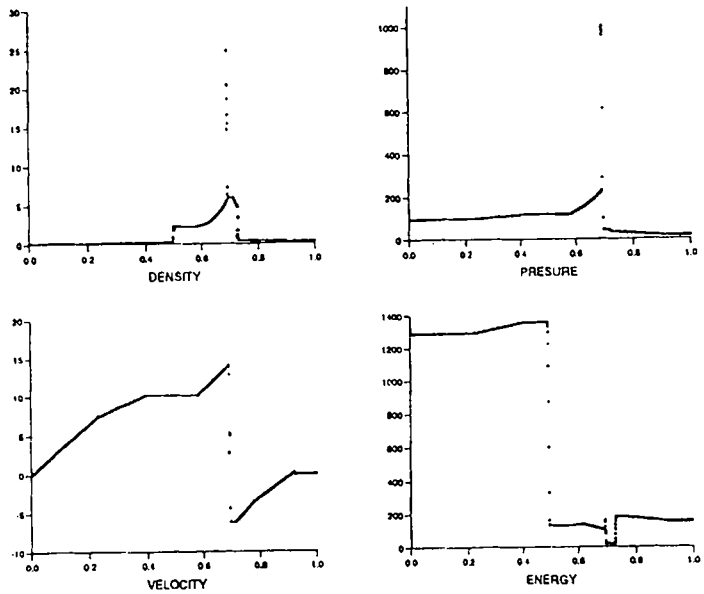

Figure 11. Blast wave problem by fourth-order scheme with FD4B limiter

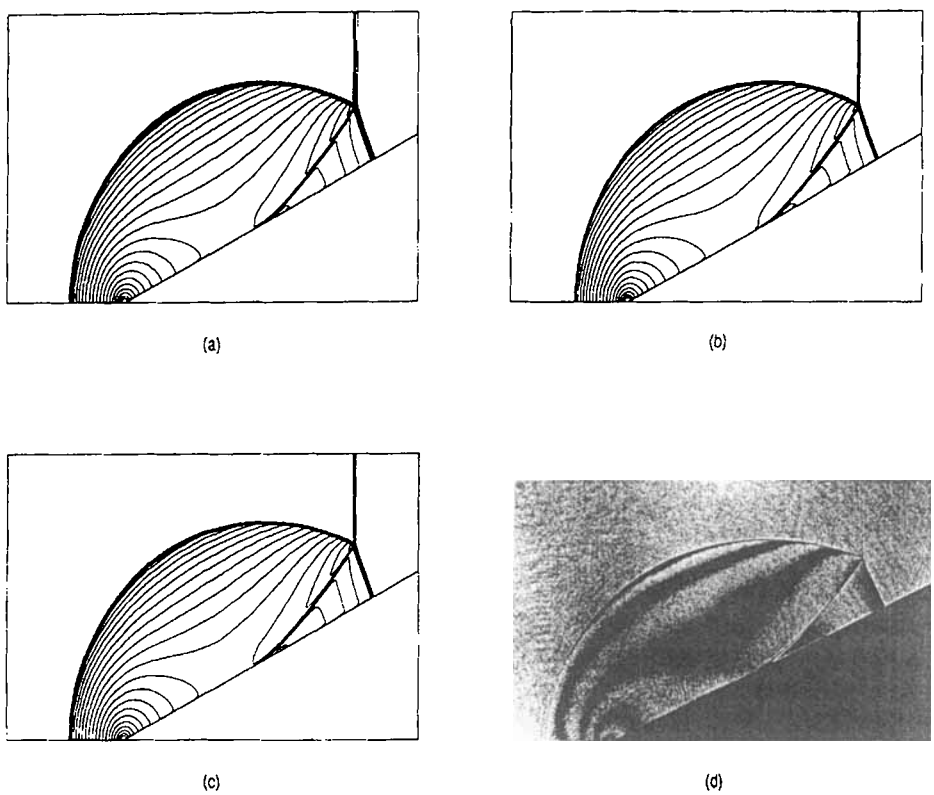

Figure 12. Shock reflection over 25° wedge: (a) computed result by second-order scheme with FD2A limiter; (b) computed result by third-order scheme with FD3A limiter; (c) computed result by fourth-order scheme with FD4A limiter; (d) experimental result

5.4. Shock reflection problem

To illustrate the capability of our schemes to solve multidimensional problems, we computed solutions to the time-dependent, two-dimensional Euler equations that simulate the flow resulting from the reflection of shock wave at Mach number 1·7 from a wedge at an angle of 25° to the incident flow.

A hybrid scheme involving the linearized solver and an exact solver used adaptively was applied. Figure 12 shows a comparison between the numerical solutions obtained by (a) the second-order scheme with the FD2A limiter, (b) the third-order scheme with the FD3A limiter, (c) the fourth-order scheme with the FD4A limiter and (d) the experimental result (courtesy of Professor K. Takayama, Shock Wave Research Center, Tohoku University, Sendai, Japan). Good agreement is seen between the numerical and experimental results.

6. CONCLUSIONS

In this paper we have discussed a way to extend the fully discrete high-resolution schemes introduced in References 1 and 2 to systems of non-linear hyperbolic conservation laws. Second-, third- and fourth-order high-resolution schemes for non-linear systems are presented. These schemes are tested and validated by solving the one- and two-dimensional Euler equations of gas dynamics for some well-known test problems. The computation was carried out using two different kinds of approximate Riemann solvers which satisfy the entropy condition. The numerical solutions show that these high-resolution schemes can give very satisfactory performance.

REFERENCES

1. J. Shi and E. F. Toro, 'Fully discrete arbitrary-order schemes for a model hyperbolic conservation law', College of Aeronautics Report no. 9307, Cranfield University, 1993.
2. J. Shi and E. F. Toro, 'Fully discrete high-order shock-capturing numerical schemes', *Int. j. numer. methods fluids.*
3. S. K. Godunov, 'A difference scheme for numerical computation of discontinuous solution of hydrodynamic equations', *Math. Sbnornik, 47, 271–306 (1959) (in Russian); Engl. transl. U.S. Joint Publ. Res. Service, JPRS 7226, 1959.*
4. G. Strang, 'On the construction and comparison of difference schemes', *SIAM J. Numer. Anal.*, **5**, 506–517 (1968).
5. P. L. Roe, 'Approximate Riemann solvers, parameter vectors, and difference schemes', *J. Comput. Phys.*, **43**, 357–372 (1981).
6. B. Engquist and S. Osher, 'One-side difference approximates for nonlinear conservation laws', *Math. Comput.*, **36**, 321–52 (1981).
7. P. L. Roe, 'Some contributions to modelling of discontinuous flows', in *Lectures in Applied Mathematics*, Vol. 22, American Mathematical Society, Providence, RI, 1985.
8. A. Harten and J. M. Hyman, 'Self-adjusting grid methods for one-dimensional hyperbolic conservation laws', *J. Comput. Phys.*, **50**, 235–269 (1983).
9. B. Einfeldt, C. D. Munz, P. L. Roe and B. Sjogreen, 'On Godunov-type methods near low densities', *J. Comput. Phys.*, **92**, 273–295 (1991).
10. E. F. Toro, 'A linearized Riemann solver for the time dependent Euler equations of gas dynamics', *Proc. R. Soc. Lond. A*, **434**, 683–693 (1991).
11. G. Sod, 'A survey of several finite difference methods for systems of nonlinear hyperbolic conservation laws', *J. Comput. Phys.*, **27**, 1–31 (1978).
12. P. Woodward and P. Colella, 'The numerical simulation of two-dimensional fluid flow with strong waves', *J. Comput. Phys.*, **54**, 115–173 (1984).